Comparison of SSH anomalies derived from open-ocean bottom pressure measurements (from NOAA DART® systems) with multi-satellite merged altimeter missions and coastal tide gauge records

George Mungov[1] and Yongsheng Zhang[2]

[1]CU/CIRES and NOAA/NCEI, Boulder, Colorado, USA

[2]CICS-MD and NOAA/NCEI, Silver Springs, Maryland, USA

Introduction

The purpose of this study is to investigate the possible application of NOAA DART® (Deep-ocean Assessment and Reporting of Tsunamis) data beyond tsunami research. We compare DART® data with coastal tide gauge observations and satellite altimeter records. NOAA DART® systems have been in operational use since 2005, following about 20 years of development and testing – Gonzalez et al, (2005), Mofjeld (2009), Bernard and Meinig (http://paroscientific.com/pdf/140%20DART_History%20with%20notes.pdf). The full 39-station network was completed in 2008 and now it is functioning under the US National Tsunami Hazards Mitigation Program (Folger, 2015). DART® systems are designed to measure the changes in the water column pressure at the ocean floor caused by passing tsunamis and send the data to tsunami warning centers. Currently in use are DART® systems second generation (DART® II) - https://www.ndbc.noaa.gov/dart/dart.shtml. Their significant feature is two-directional communication via Iridium satellite system between the moored surface buoys and NOAA land-based operational centers: the National Data Buoy Center (NDBC) and two Tsunami Warning Centers (TWCs) in Hawaii and Alaska. The communication between the bottom pressure recorders (BPR) on the sea floor and the surface buoys is through acoustic channel. DART® II systems can be put in different recording and transmitting modes in two ways: autonomously by changes in water pressure exceeding a threshold value; and remotely by the operators in the warning centers – Meinig et.al (2005). In general, tsunamis are generated by earthquakes, volcanoes, landslides, or sudden significant changes in atmospheric pressure (meteotsunamis). Most tsunamis are triggered by earthquakes. Earthquakes are effectively monitored worldwide. Information about the location and the magnitude of recent earthquakes is distributed within a minute of their occurrence. This information, however, is not sufficient for tsunami forecasting as it does not include any information about the tsunami source area, which is what determines the magnitude of the generated tsunami. Depending on several factors, an earthquake may or may not generate a tsunami. DART® in-situ measurements are the only reliable indicator for generated tsunamis and their magnitude. For this reason, the DART® system is considered one of the most important components of the tsunami warning system in the Pacific and Atlantic oceans and in the Caribbean Basin. Along with the confirmation for generated tsunamis,

1

recorded tsunami wave forms are used to estimate the tsunami source parameters via inversion techniques proposed by Prof. Kenji Satake (Satake, 1987, 1989). After receiving reliable estimation of the tsunami source parameters—the uplift area and uplift heights and timing—these parameters are used in tsunami numerical models for precision forecasting of tsunami wave propagation, arrival times, and heights of tsunami waves along affected coasts. DART® data are also applied for tsunami model calibration and coastal zone risk assessments. During recent years, the inversion techniques were upgraded with the application of data assimilation methods (Maeda et al., 2015). A significant advance has been the joint assimilation of DART®, coastal tide gauge, GPS and remote sensing data. This is described in Blewitt et. al. (2009) for the use of GPS data for real-time earthquake source determination, Wang et. al. (2018) for assimilation of DART® and coastal tide gauge data, Wang et. al. (2019) for assimilation of dense observational network data, Mulia et. al. (2020) for assimilation of DART® and remote sensing data, Jakir et. al. (2020) for assimilation of shipborne GNSS data, etc. All of these studies and the corresponding developed methods use open-ocean DART® observations as a key element.

Detailed descriptions of the DART® system can be found on the web pages of the National Center for Tsunami Research (https://nctr.pmel.noaa.gov/Dart/dart_overview.html), National Data Buoy Center (https://www.ndbc.noaa.gov/dart/dart.shtml), and Gonzalez et. al. (2005). DART® systems use the Paroscientific submersible depth sensor (http://www.paroscientific.com/pdf/D50_Series_8000.pdf). The sensor is placed in an alloy container fixed on the ocean floor at depths between 4000 and 6000 meters (https://www.ndbc.noaa.gov/dart/dart.shtml). Due to the high water pressure, the alloy containers start experiencing plastic deformations, and long-term water pressure variations are not recorded.

As we stated earlier, DART® data are now used in tsunami research and forecasting, employing relatively short time segments lasting from several hours to several days. To investigate the time scales where DART® observations reliably represent open-ocean water level variations in our study, we compare 17 DART® records against satellite altimeter and coastal tide gauge observations.

DART®, satellite altimeter and coastal tide gauge data

The NOAA National Centers for Environmental Information in Boulder, Colorado (NCEI-CO), is the archive for high-resolution water-level data as part of the US National Tsunami Hazards Mitigation Program. NCEI Hazards Group manages an archive of almost 300 DART® records covering a period of 20+ years, including the pre-DART® era deployments - https://www.ngdc.noaa.gov/hazard/DARTData.shtml. We selected 17

DART® stations from the NCEI archive with long and quality records from all geographic areas in the Pacific and Atlantic oceans, Gulf of Mexico and the Caribbean Basin (Figure 1 and Table 1).

NCEI Hazards group also manages the long-term archive for all NOAA coastal tide gauge data: 1-minute water level data from the NOAA/NOS Center for Operational Oceanographic Products and Services (CO-OPS), and high-resolution water level data from the Pacific Tsunami Warning Center (PTWC) and the National Tsunami Warning Center (NTWC) - https://www.ngdc.noaa.gov/hazard/tide.shtml. From this archive and from international sources, we selected several island and coastal stations – Figure 1. The selection criteria for these stations were as follows: they had to be close to the selected DART® stations, located on isolated islands or, when not available, on open continental coasts, and with high data quality. Data providers include:

- NOAA/NOS/CO-OPS records: 13 from Pacific islands, Alaska, Bermuda Islands, and Caribbean Basin

- UNAM (Mexico) provided data for the Acapulco coastal tide gauge

- SHOM (France) provided data for Clipperton Island (France)

- Data for Quepos (Costa Rica), St. Cruz (Galapagos Island, Ecuador), Kushiro (Japan), and Nuku'lofa (Tonga) were extracted from the IOC Sea Level Monitoring Facility (http://www.ioc-sealevelmonitoring.org).

DART® records represent the sum of the weight of the water column above the BPR and the atmospheric pressure at the ocean surface. Atmospheric pressure as gridded field data over the Pacific and Western Atlantic was provided by NOAA/OAR/Physical Science Laboratory NOAA-CIRES-DOE 20th Century Reanalysis (https://www.psl.noaa.gov/data/gridded/data.20thC_ReanV3.html), where the time step is 3 hours. Currently this reanalysis goes up to 2015 only. Here it should be mentioned that when investigating tsunamis it is not necessary to apply atmospheric pressure correction, because for such short periods (less than 24 hours) the effect of atmospheric pressure variations is negligible.

In the present study we are using daily time series multi-satellite merged sea surface height anomalies (SSHA) picked from the 1/4 degree gridded optimal interpolated daily sea level anomaly (https://coastwatch.noaa.gov/cw/satellite-data-products/sea-surface-height/sea-level-anomaly-and-geostrophic-currents-multi-mission-global-optimal-interpolation-gridded.html) – Leuliette and Scharroo (2010). In previous versions, satellite altimeter data were extracted from NASA/JPL PO.DAAC merged SSHA with a time step of 5 days, with no interpolation for intermediate days that provided an approximate comparison with DART® data.

Data processing

3

DART® and island and coastal tide gauge records are processed (which involves quality control, de-spiking, and de-tiding) as described in Mungov et al (2012). Special attention was paid to fix the drifts in the records composed by initial exponential segment, with length between two days and two weeks, followed by a linear or close to linear trend along the rest of the record. This phenomena is described by Paros and Kobayashi (http://paroscientific.com/pdf/G8101_Root_Causes_of_Quartz_Sensors_Drift.pdf). posted on the Paroscientific web site. Initial exponential segments are approximated with higher-order polynomial functions, and trends in the following segments are approximated with linear relationships.

All DART® records were decimated to one hour time series, and the residuals from the individual deployments were centered to one common level. These new long records are considered homogeneous as all deployments are very close to each other because we are looking at larger-scale processes. Daily mean values were taken as an arithmetic mean for consistency with satellite altimeter sea level anomalies (SLA) and coastal tide gauge records.

Atmosphere pressure time series are extracted for the centers of the 1/4 degree grids where the 17 selected DART® stations are located. Atmosphere pressure time series are interpolated to reach a 1-hour time step. Residuals corrected for the variations of the atmospheric pressure at the ocean surface are known as "adjusted residuals," and we get them using standard inverse barometric correction - Pugh (1987). The relationship we use is the same used in the Jason-3 Products Handbook (CNES, EUMETSAT, JPL, NESDIS. 2018), page 56:

$$inv\_bar\_corr = -9.948 \, (P_{atm} - 1013.3)$$

Tide gauge data had different time steps of 1 minute, 6 minutes and 1 hour. All records were decimated to 1 hour time step and they were quality controlled and cleaned from instrumental issues. The residuals were obtained after applying tidal analysis, and daily mean values were estimated for all records.

Verification of DART® data against multi-satellite merged sea surface height anomalies

As noted earlier, this study uses daily time series data multi-satellite merged sea surface height anomalies (SSHA) picked from the 1/4 degree gridded optimal interpolated daily sea level anomaly (https://coastwatch.noaa.gov/cw/satellite-data-products/sea-surface-height/sea-level-anomaly-and-geostrophic-currents-multi-mission-global-optimal-interpolation-gridded.html). The daily mean time series are obtained from all available satellite missions. The repeat period for the crossover points for Jason satellites is 5 days.

4

Figure 1. Used DARTs, islands and coastal tide gauge stations.
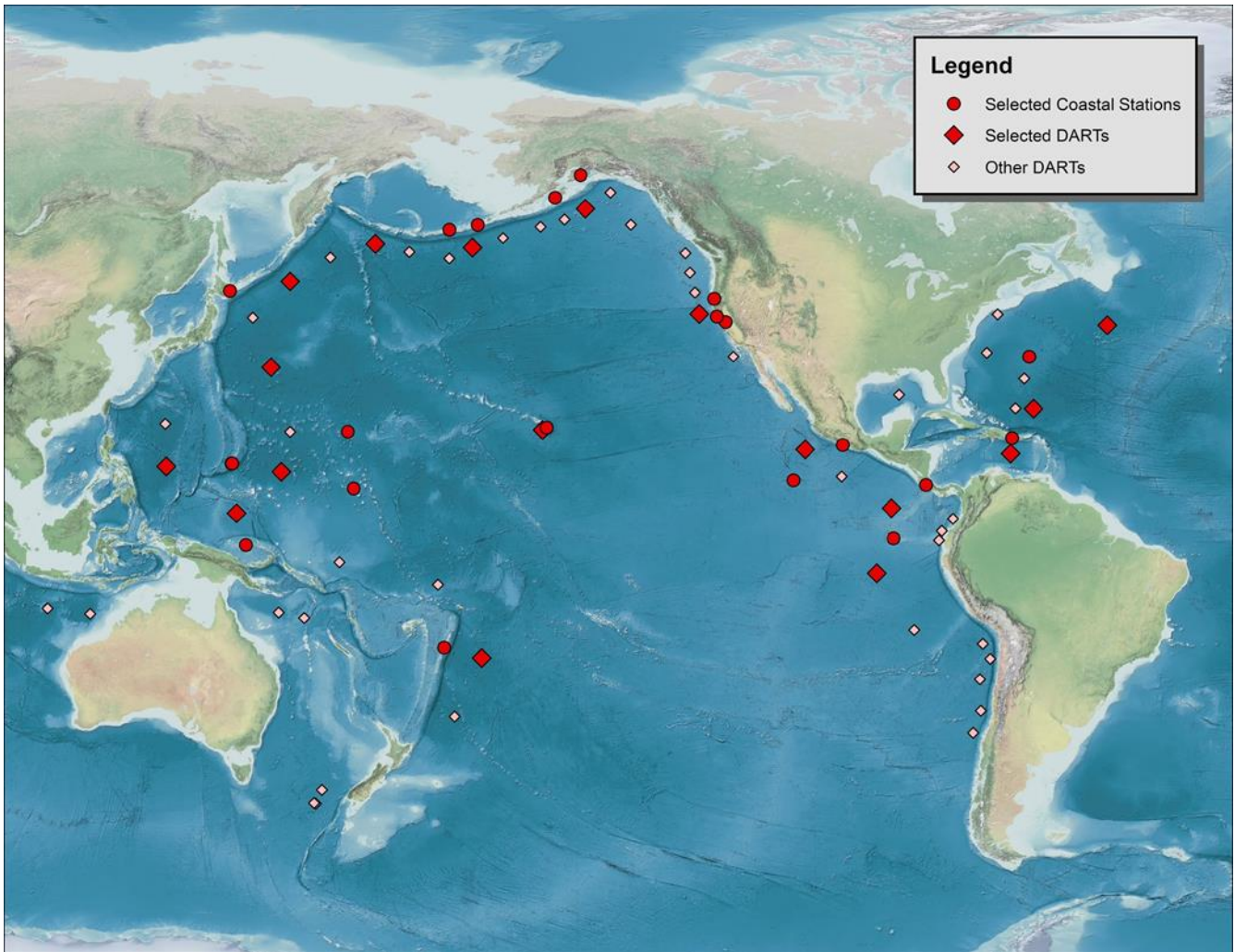
Table 1 Selected DART® stations and corresponding island and coastal tide gauges

Used DART stations				Used Island/Coastal tide gauges		
DART	Approximate location	Latitude	Longitude	Island/Coastal station	Latitude	Longitude
NE Pacific close to Japan Islands						
21413	700 NM ESE of Tokyo, JP	30.580	152.099	**Wake I.,**	19.290	166.618
21415	175 NM South of Attu, AK	50.176	171.849	**Atka, AL,**	52.232	-174.173
21419	209 NM SE of Kuril Is	44.455	155.735	**Kushiro, Japan**	42.967	144.383
North Pacific close to Aleutian Islands and US Alaska Pacific coast						
46408	212 NM South of Umnak Is, AK	49.623	-169.848	**Nikolski, AL**	52.941	-168.871
46409	210 NM SE of Kodiak, AK	55.301	-148.495	**Seaward, AL** **Alitak, AL**	60.120 56.897	-149.427 -154.248
East Pacific, off US and Mexico Pacific coasts						
46411	150 NM West of Mendocino Bay, CA	39.329	-127.010	**Port Chicago** **Arena Cove** **Crescent City**	38.0560 38.9146 41.7456	-122.0395 -123.7111 -124.1844
43412	240 NM SW of Manzanillo, MX	16.031	-107.000	**Acapulco, MX** **Clipperton, FR (2011/08 – 2012/10)**	16.838 10.280	-99.9033 -109.222
32411	710 NM WSW of Panama City, Panama	5.000	-90.686	**Quepos, Coasta Rica**	9.425	-84.172
32413	1000 NM WNW of Lima, Peru	-7.400	-93.499	**Santa Cruz, Galapagos**	-0.755	-90.313
Central Pacific - off Hawaii Islands						
51407	34 NM West of Kailua-Kona, HI	19.578	-156.586	**Kawaihae, HI**	20.037	-155.829

5

West Central Pacific					
51426	400 NM SE of Tonga	-23.007	-168.111	**Nuku'alofa, Tonga**	-21.133	-175.167
52402	540 NM ESE of Saipan	11.882	154.104	**Kwajalein. HI**	8.732	167.736
52403	345 NM North of Manus Is, New Guinea	4.052	145.608	**Lombrum, PNG**	-2.042	147.374
52405	725 NM West of Agana, Guam	12.884	132.317	**Apra Harbor, Guam**	13.439	144.654
				Pago Bay, Guam	13.428	144.797
Caribbean basin and West Atlantic (Bermuda)					
41421	300 NM North of St Thomas, Virgin Is	23.398	-63.904	**Mona Island**	-67.939	-67.939
42407	230 NM SW of San Juan, PR	15.256	-68.236	**Caja de Muertos, PR**	17.887	-66.528
				Lime Tree, PR	17.695	-64.754
44401	790 NM NNE of Bermuda	37.551	-49.986	**St. Georges I., Bermuda**	32.373	-64.703

For the days between, all available observations from other satellite missions are used or the intermediate points are obtained on a time segment of -10 days to +10 days using a temporal correlation length scale as described in Jacobs et al. (2001). Time series plots of DART® adjusted residuals and merged altimeter SSH anomalies are represented in Figure 2. The strong high-frequency oscillations in the adjusted DART® residuals are due to similar high-frequency oscillations in the atmospheric pressure data. For this reason, it was necessary to smooth adjusted DART® residuals with a 5-day running average.

Figure 2. DART® adjusted daily mean residuals and merged altimeter SSHA. DART® adjusted SSHA – blue lines, 5 days smoothed DARTs adjusted SSHA - read lines, altimeter SSHA - black lines. For consistency we keep same vertical and horizontal scales everywhere.

Aleutian Islands, North Pacific

DART® 46408   DART® 46409

North West Pacific, off the coasts of Japan   **US West Coast**

DART® 21415   DART® 46419

6
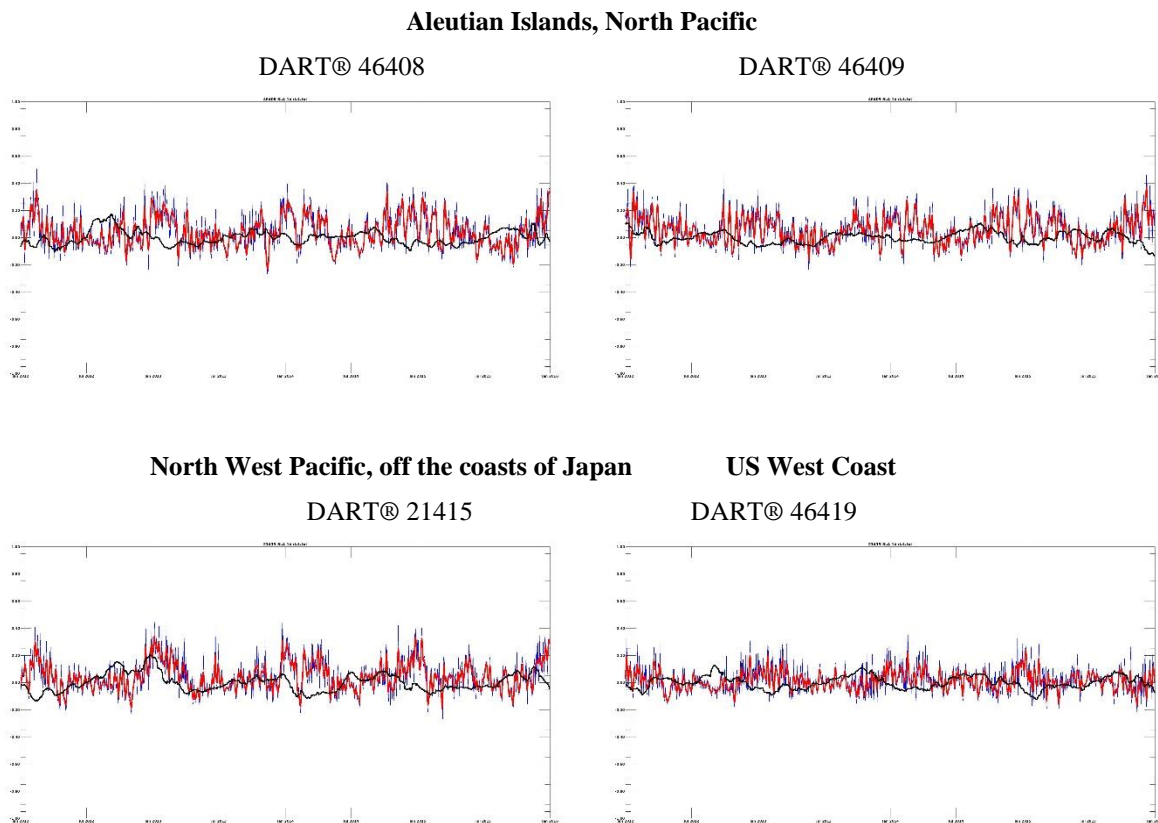
Central Pacific – off Hawaii Islands

DART® 51407
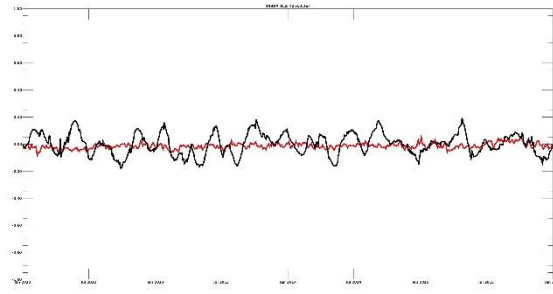
Central West Pacific
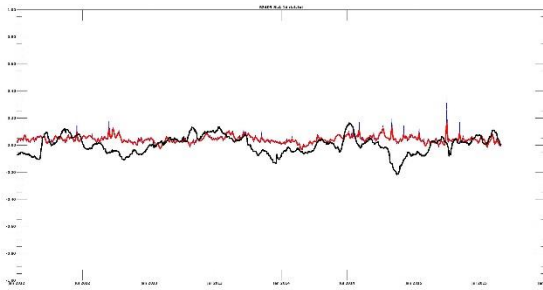
### DART® 52405

Central East Pacific

DART® 43412
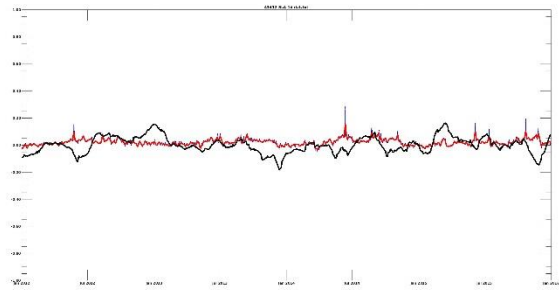
### DART® 52403
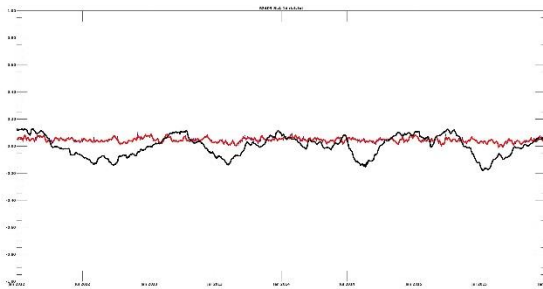
### DART® 32411

South Pacific

DART® 51426


7
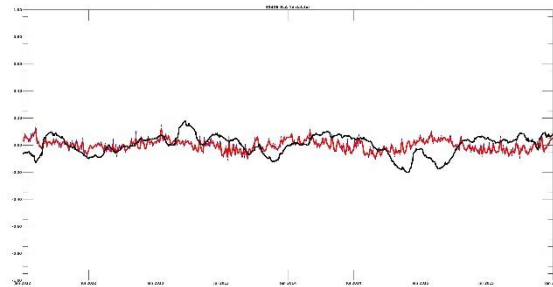
Atlantic Ocean

Off US East Coast DART® 44401   North of US Virgin Islands DART® 41421
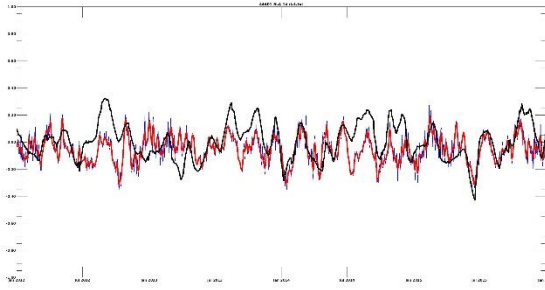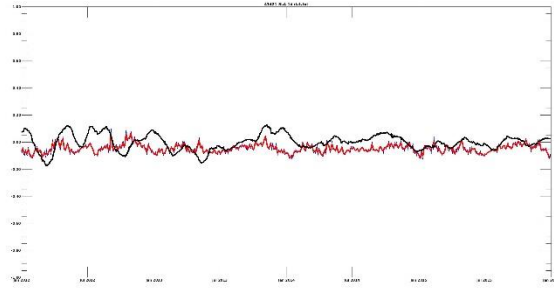

Caribbean basin

DART® 42407
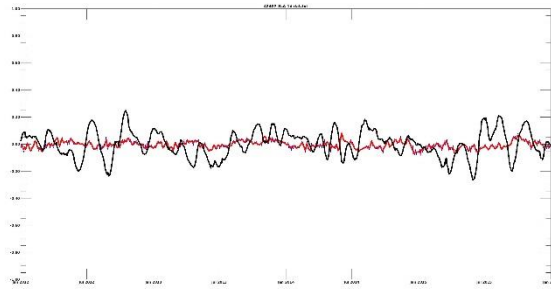
The analysis of the plots reveals that adjusted DART® SSHA and altimeter SSHA are in very good agreement for the West Atlantic (off East US coast) DART® 44401 (44403) and the North West Pacific off the Japan Islands. The very intensive atmospheric processes into the synoptic time scale are a common feature of these regions. For all other regions, altimeter SSHA represent the seasonal dynamics in the ocean topography, while DART® SSHA could be used for representing sub-scale variations not existing in altimeter data. Energy spectra of DART® adjusted daily SSHA, 5 days smoothed DART® adjusted SSHA and merged altimeter SSHA are presented in Figure 3 along with the frequency coherence function between DART® 44401 and altimeter SSHA.

Figure 3. Spectra of DART® adjusted daily SSHA – blue lines, 5 days smoothed DART® adjusted SSHA – red lines, altimeter SSHA - black lines.

Aleutian Islands, North Pacific

DART® 46408   DART® 46409

8
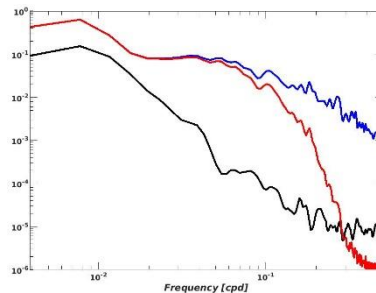
## North West Pacific, off the coasts of Japan
DART® 21419
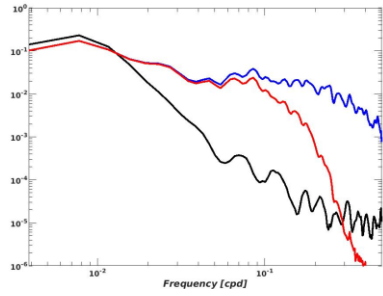
US West Coast
DART® 46411
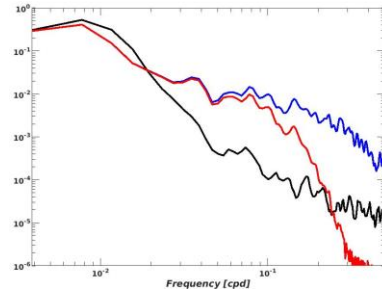
Central West Pacific
DART® 52405
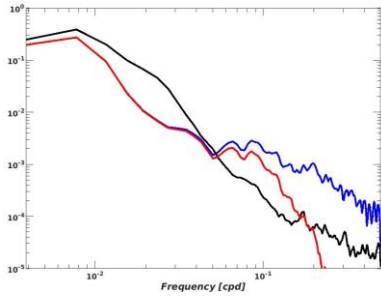
Central Pacific
DART® 51407
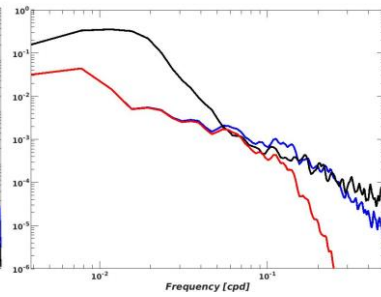
Central East Pacific
### DART® 32413
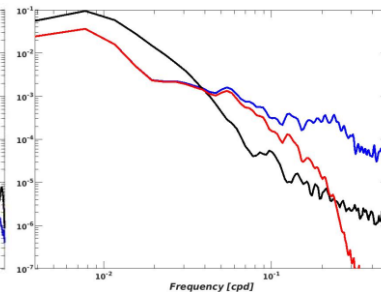
South Pacific
DART® 51426
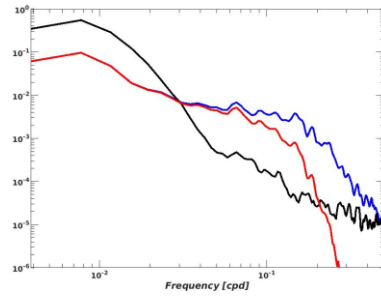

Atlantic Ocean

### North West Atlantic
DART® 44401 (44403)


North of US Virgin Islands
DART® 41421

9
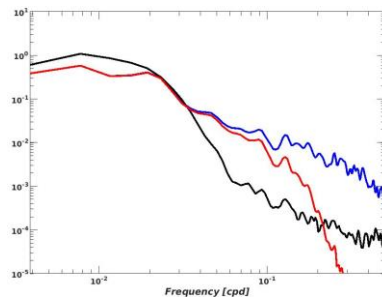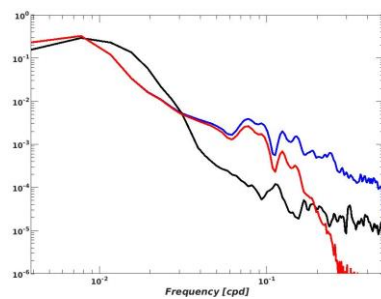
Coherence
DART® 44401 – altimeter SSHA
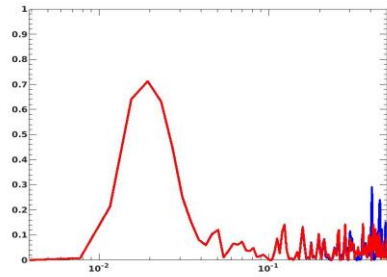
Caribbean basin
DART® 42407
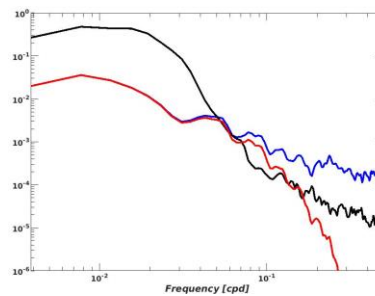
Investigating the power spectra, we see one general feature – the energy of the altimeter spectra is higher at lower frequencies, and after the peak the energy decreases almost linearly towards higher frequencies. We explain this behavior by noting the fact that although the time step of altimeter SSHA is one day, the repeating cycle of Jason's satellites at crossover points is 5 days and the contribution of other satellite data is not sufficient to reveal the short period variations that are available in DART® records or the averaging between several altimeter data that is smoothing/smashing these variations. As a result altimeter SSHA on time series plots look "smoothed" with no short-period oscillations as seen in DART® records. The benefit of this analysis is that DART® and altimeter records could be used in parallel as DART® data discover the "fine" or high-frequency components while altimeter data reveal low-frequency components - mostly the seasonal variations. Of course this is only possible in the vicinity of DART® deployments.

Verification of DART® data against island/coastal tide gauge data

When comparing DART® adjusted SSHA with coastal or island tide gauge record, it is necessary to consider several facts.

- These tide gauges are not located close to DART® deployments. For this reason, if the distance between the DART® deployment site and the tide gauge is very big, the two types of records could have different features (i.e., different behavior).
- Coastal tide gauges are significantly influenced by local topographic features, such as the dimensions of the continental/island shelf. Also, as a general practice, tide gauges are installed in ports or inside bays, which contributes to additional amplification of the recorded water levels during storms, local seiches, etc.
- As we are looking for tide gauge records worldwide, from any available international sources, the quality of the data differs significantly. This is true of records from different sources, as well as of records from a single tide gauge, which can experience significant changes in data quality over time.

10

- As a result of all of these circumstances, for every one DART® record we tried to select the "best match" from several alternatives (Table 1).

Without going into details, as this part of the study is not directly relevant to the scope of the OSTST meeting, next we briefly outline our main conclusions.

- Some of the coastal records experience strong influence from local topographic conditions, sometimes resulting in very strong high-frequency oscillations. These oscillations need smoothing.
- We found that there is a good match between DART® adjusted SSHA and coastal or island tide gauge record in regions with high atmospheric dynamic. These regions are the same revealed in the previous section: the North Pacific Ocean and, surprisingly, the Caribbean Basin and around the Hawaii Islands. We believe that this is due to the fact that in the last cases, matching tide gauges are located on islands located away from continents with good data, and the distance to the relevant DART® deployment sites is not too big.
- For all these cases, the maximum coherence was in the range of 0.30 – 0.35 (0.52 for Caribbean DART 42407 and Lime Tree Bay at US Virgin Islands) for frequency band one cycle per 7 to 12 days. For frequencies lower than one cycle per 12-14 days and for frequencies higher than one cycle per 5-7 days, the coherence very quickly tends to 0.
- The frequency band one cycle per 7 to 12 (14) days could be considered as a representative for DART® adjusted SSHA. For lower frequencies, DART® systems do not record the long-period pressure variations due to BPR container plastic deformations. For frequencies higher than 1 cycle per 5-7 days, local conditions at DART® deployment sites and at the coastal stations are dominating, along with the effect of smoothing the high-frequency oscillations in the coastal and DART® adjusted SSHA.

Next, in Figure 4, we present plots of time series, spectra and coherence functions for selected DARTs® and corresponding tide gauges.

Figure 4. Time series, spectra and coherence plots for selected DART® adjusted SSHA – blue lines, smoothed DARTs adjusted SSHA – red lines, and island/coastal tide gage residuals – black lines.

11

North Pacific: Time series plots for DART 21415 and 9461710 Atka, Alaska for 2012 - 2015
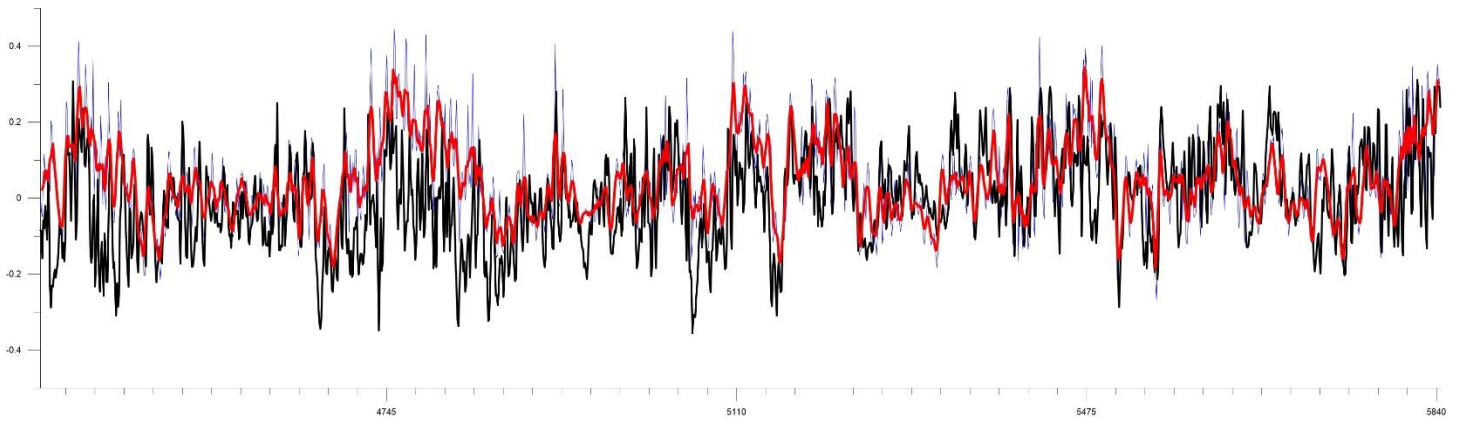
Spectra and coherence for DART 21415 and 9461710 Atka, Alaska
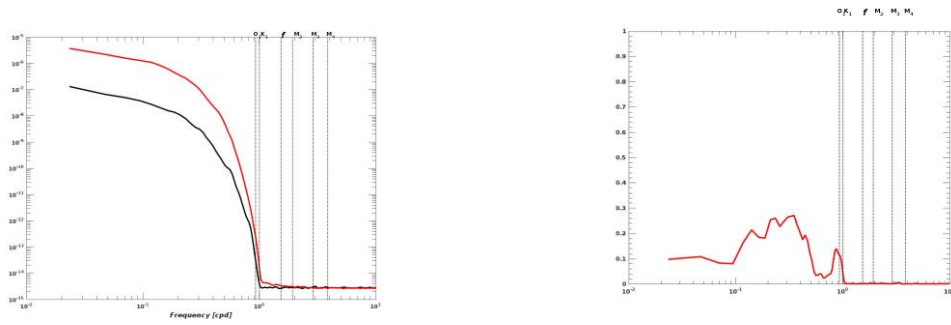
Central Pacific, Hawaii: Time series plots for DART 51407 and tide gauge Kawaihae, HI, USA for 2012 - 2015
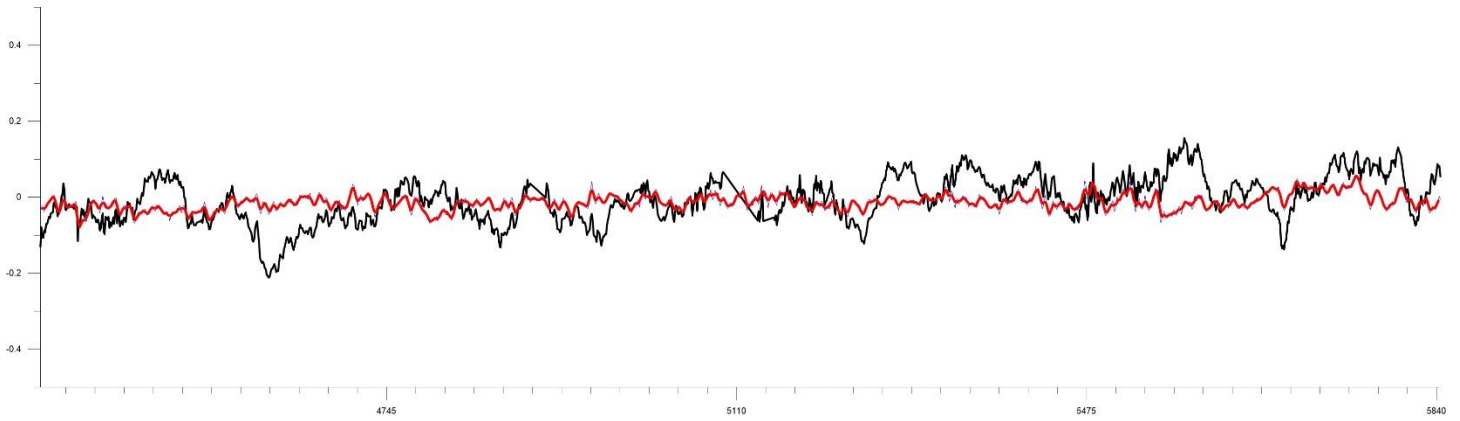

Spectra and coherence for DART 51407 and tide gauge Kawaihae, HI, USA

12

Caribbean basin: Time series plots for DART 42407 and tide gauge Lime Tree Bay at US Virgin Islands for 2012 - 2015
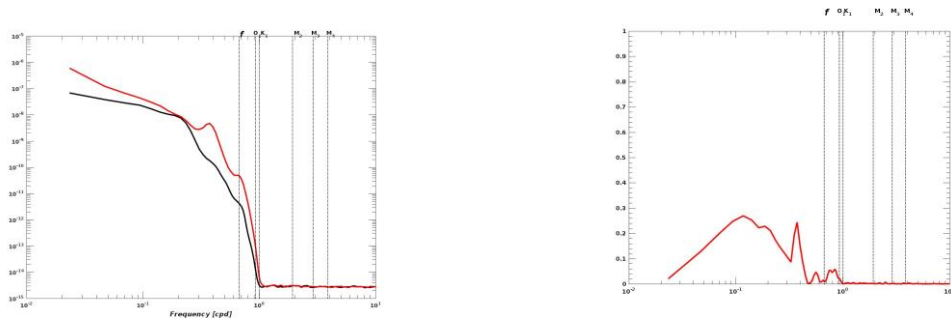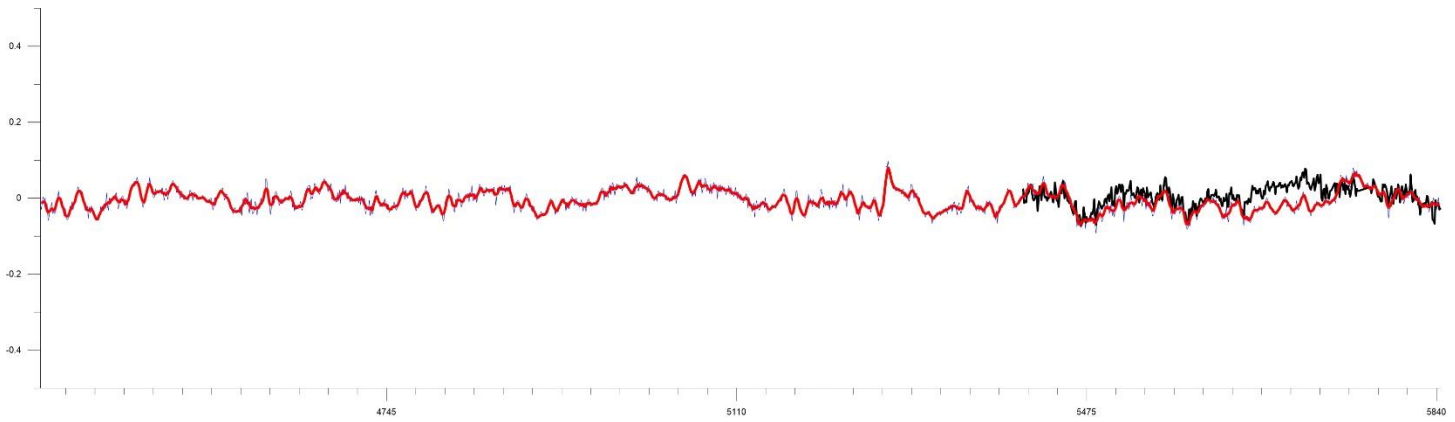
Spectra and coherence for DART 42407 and tide gauge Lime Tree Bay at US Virgin Islands
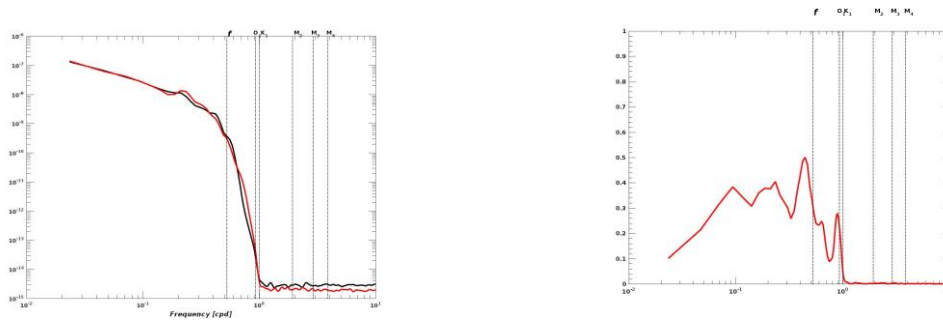
Conclusions

We found that there is a good match between DART® adjusted SSHA with altimeter SSHA and coastal or island tide gauge records in regions with high atmospheric dynamics. These regions are: the North Pacific Ocean along Japan and the Aleutian Islands and Alaska; around the Hawaii Islands; the West Atlantic off the US East Coast, and the Caribbean Basin. Our findings indicate that in these regions DART® adjusted SSHA characterize the open-ocean water level variations in the frequency band one cycle per 7 to 12 (14) days. For lower frequencies (periods longer than 1 cycle per 12-14 days), DART® systems do not record the long-period pressure variations due to BPR container plastic deformations. For frequencies higher than 1 cycle per 5-7 days, local conditions at DART® deployment sites and at the coastal stations are dominating along with the effect of the smoothing the high-frequency oscillations in the coastal and DART® adjusted SSHA.

The smoothed pattern of altimeter SSHA indicates that this behavior is determined by the 5-day repeating cycle of Jason's satellites at crossover points, as the involvement of other satellite data does not contribute to the revealing of the short period variations that are available in DART®. But at the same time, DART® and altimeter records could be used in parallel as DART® data discover the "fine" or high-frequency components while altimeter data represent low-frequency components, such as seasonal variations.

13

References

Blewitt, G., Hammond, W.C., Kreemer, C. et al. (2009) GPS for real-time earthquake source determination and tsunami warning systems. J Geod 83, 335–343 (2009). https://doi.org/10.1007/s00190-008-0262-5

Bernard, E., and C. Meining. History and future of deep-ocean tsunami measurements. http://paroscientific.com/pdf/140%20DART_History%20with%20notes.pdf. Accessed on August 2020.

CNES, EUMETSAT, JPL, NESDIS. 2018. Jason-3 Products Handbook, Sept 2018, 71 p. https://www.ospo.noaa.gov/Products/documents/hdbk_j3.pdf

Folger, P. 2015. The U.S. Tsunami Program: A Brief Overview. Congressional Research Service 7-5700. www.crs.gov, R41686

González F. I., E. Bernard, C. Meinig , M. Eble, H. Mofjeld, S. Stalin. (2005) The NTHMP Tsunameter Network, Natural Hazards, Springer, vol. 35(1), pages 25-39, May.

González, F.I., V.V. Titov, H.O. Mofjeld, A. Venturato, S. Simmons, R. Hansen, R. Combellick, R. Eisner, D. Hoirup, B. Yanagi, S. Yong, M. Darienzo, G. Priest, G. Crawford, and T. Walsh (2005): Progress in NTHMP

hazard assessment. Nat. Hazards, 35(1), Special Issue, U.S. National Tsunami Hazard Mitigation Program, 89–110.

Gusman, A., Sheehan, A., and Satake, K. (2020) Improving tsunami forecast with data assimilation on dense pressure gauge arrays: the 2009 Dusky Sound, New Zealand, tsunami, EGU General Assembly 2020, Online, 4–8 May 2020, EGU2020-11411, https://doi.org/10.5194/egusphere-egu2020-11411, 2020

Jacobs, G., Barron, C., Rhodes, R. (2001). Mesoscale characteristics Journal of Geophysical Research: Oceans 106(C9), 19581-19595. https://dx.doi.org/10.1029/2000jc000669

Jakir M. H., I. E. Mulia , D. , A. F. Sheehan (2020) Data Assimilation for Tsunami Forecast with Shipborne GNSS Data in the Cascadia Subduction Zone. CU CIREZ Rendezvous 2020.
https://insidecires.colorado.edu/rendezvous/uploads/Rendezvous_2020_7748_1597254956.pdf

Leuliette, E. W., and R. Scharroo (2010). Integrating Jason-2 into a Multiple-Altimeter Climate Data Record. Marine Geodesy, 33(1), 504–517. doi:10.1080/01490419.2010.487795

Mofjeld, H.O. (2009), Tsunami measurements. In The Sea, Volume 15: Tsunamis (eds. A. Robinson and E. Bernard), (Harvard University Press, Cambridge, MA, 2009) pp. 201–235.

Maeda, T., Obara, K., Shinohara, M., Kanazawa, T., & Uehira, K. (2015). Successive estimation of a tsunami wavefield without earthquake source data: A data assimilation approach toward real-time tsunami forecating. Geophysical Research Letters, 42, 7923–7932. https://doi.org/10.1002/2015GL065588

Meinig, C., S.E. Stalin, A.I. Nakamura, H.B. Milburn (2005), Real-Time Deep-Ocean Tsunami Measuring, Monitoring, and Reporting System: The NOAA DART® II Description and Disclosure. NCTR,
https://nctr.pmel.noaa.gov/Dart/Pdf/DART_II_Description_6_4_05.pd

Mulia, I.E., Hirobe, T., Inazu, D. et al. Advanced tsunami detection and forecasting by radar on unconventional airborne observing platforms. Sci Rep 10, 2412 (2020). https://doi.org/10.1038/s41598-020-59239-1

Mungov, G., Eble´, M., & Bouchard, R. (2013). DART® tsunameter retrospective and real-time data: A reflection on 10 years of processing in support of tsunami research and operations. Pure and Applied Geophysics, 170, 1369–1384. doi:10.1007/s00024-012-0477-5.

NOAA-CIRES-DOE 20th Century Reanalysis Version 3 completed 1836-2015: early evaluation initiation. NOAA, ESRL, Boulder, Colorado.

Paros, J. M., and T. Kobayashi. Root causes of Quartz Sensor Drift. Paroscientific, Technical Note, Doc. No. G8101 Rev. A. http://paroscientific.com/pdf/G8101_Root_Causes_of_Quartz_Sensors_Drift.pdf

Pugh, D. T. 1987. Tides, surges and mean sea-level. Natural Environmental Research Council, Swindon, UK.

Satake, K. 1987. Inversion of tsunami waveforms for the estimation of a fault heterogeneity: Method and numerical experiments. Journal of Physics of the Earth, 35, 241–254

Satake, K. 1989. Inversion of tsunami waveforms for the estimation of heterogeneous fault motion of large submarine earthquakes: The 1968 Tokachi-oki and 1983 Japan Sea earthquakes. JGR, Solid Earth, vol. 94, issue b5, 5627-5636. https://doi.org/10.1029/JB094iB05p05627

Wang, Y., Satake, K., Maeda, T. et al. (2018) Data assimilation with dispersive tsunami model: a test for the Nankai Trough. Earth Planets Space 70, 131. https://doi.org/10.1186/s40623-018-0905-6

Wang, Y., Maeda, T., Satake, K., Heidarzadeh, M., Su, H., Sheehan, A. F., & Gusman, A. R. (2019). Tsunami data assimilation without a dense observation network. Geophysical Research Letters, 46. https://doi.org/10.1029/2018GL080930